BBA - Molecular Basis of Disease 1868 (2022) 166320

Contents lists available at ScienceDirect

BBA - Molecular Basis of Disease

journal homepage: www.elsevier.com/locate/bbadis

Prevotella copri ameliorates cholestasis and liver fibrosis in primary sclerosing cholangitis by enhancing the FXR signalling pathway

Baorong Jiang [a], Gehui Yuan [a], Jialin Wu [a], Qian Wu [a], Lei Li [a,b,*], Ping Jiang [a,b,*]

[a] Center for Global Health, School of Public Health, Nanjing Medical University, 101 Longmian Avenue, Nanjing, Jiangsu 211166, PR China

[b] Key Lab of Modern Toxicology of Ministry of Education, School of Public Health, Nanjing Medical University, 101 Longmian Avenue, Nanjing, Jiangsu 211166, PR China

ARTICLE INFO

Keywords:
Cholestasis
Primary sclerosing cholangitis
Microbiota
Prevotella copri
Bile acid metabolism

ABSTRACT

Primary sclerosing cholangitis (PSC) is a chronic cholestatic liver disease characterized by bile duct inflammation, fibrosis, bile acid (BA) metabolism disorders and gut microbiota dysbiosis. At present, the aetiology and pathogenesis of PSC are not clear, and there is no specific or effective treatment available. Therefore, new research perspectives are needed to explore effective methods to treat PSC and improve symptoms. The intestinal microbiota of patients with PSC is known to be significantly different from that of healthy people. By comparing differentially abundant bacterial genera in PSC patients, it was found that the abundance of *Prevotella copri* (*P. copri*) was significantly decreased, suggesting that this species may have a protective effect against PSC disease. Therefore, comprehensively exploring the role and possible function of *P. copri* in the disease process is worthwhile. In this study, a PSC mouse model was established by feeding mice a customized diet supplemented with 0.1% (w/w) 3,5-diethoxycarbonyl-1,4-dihydrocollidine (DDC) for one week, and the abundance of *P. copri* was confirmed to be decreased in this model. Previous studies in patients and animal models have demonstrated that gut microbiota intervention is an acceptable treatment for some diseases. We found that intervention with *P. copri* could significantly improve cholestasis and liver fibrosis by enhancing the FXR-related signalling pathway in PSC mice. Together, through the overall effect of *P. copri* on intestinal microbiota structure and its association with BAs, we speculate that *P. copri* intervention might be as potential biological treatment of PSC.

1. Introduction

Primary sclerosing cholangitis (PSC) is a chronic cholestatic liver disease characterized by biliary tract inflammation, fibrosis, and intrahepatic and/or extrahepatic bile duct destruction, leading to cholestasis, bile duct stenosis, and hepatic fibrosis [1–4]. Epidemiological investigation has shown that PSC occurs mostly in middle-aged men and is closely associated with inflammatory bowel disease (IBD) [5–10]. Therefore, intestinal microbiota disturbance may have a potential correlation with PSC, and intestinal microbiota plays an important role in various metabolic processes of the body. A previous study demonstrated that PSC patients have distinct gut microbial profiles compared to healthy humans [11–14]. The abundance of *P. copri* (*P. copri*) was found to be decreased in the intestinal tract of patients with PSC and PSC-IBD [12,14]. *P. copri* is the most common form of human gut bacteria in the genus *Prevotellaceae*, which is linked to diet and disease [15–18]. It has been reported that *P. copri*, as a genus of symbiotic bacteria, can produce short-chain fatty acids, which can improve the immune tolerance of a foetus, suggesting an important role of *P. copri* carried by mothers in foetal immune defence [19]. In addition, it has been shown that *P. copri* improves glucose homeostasis in Goto-Kakizaki rats with gastrointestinal resection by enhancing the bile acid (BA) metabolism signal [20]. This suggests that *P. copri* may be related to cholestasis and potentially beneficial to disease progression in PSC, but the mechanism remains unclear.

Bile acids (BAs), important components of bile, are synthesized from cholesterol in hepatocytes, and their synthesis is catalysed by cholesterol 7α-hydroxylase (*Cyp7a1*), microsomal sterol 12α-hydroxylase (*Cyp8b1*) and cholesterol 27-hydroxylase (*Cyp27a1*) [21]. A portion of primary BAs are amidated by glycine or taurine to form conjugated BAs before

Abbreviations: Prevotella copri, *P. copri*; BA, bile acid; DDC, 3,5-diethoxycarbonyl-1,4-dihydrocollidine; PSC, Primary sclerosing cholangitis; FXR, Farnesoid X receptor.

* Corresponding authors at: Center for Global Health, School of Public Health, Nanjing Medical University, 101 Longmian Avenue, Nanjing 211166, PR China.
E-mail addresses: lilei@njmu.edu.cn (L. Li), jiangping@njmu.edu.cn (P. Jiang).

https://doi.org/10.1016/j.bbadis.2021.166320
Received 15 August 2021; Received in revised form 30 November 2021; Accepted 3 December 2021
Available online 10 December 2021

being excreted into the bile and into the duodenum [22,23]. In the intestine, the gut microbiome could participate in the transformation of conjugated BAs to unconjugated BAs through multiple hydrolases and regulate the expression of rate-limiting enzymes in the BA synthesis pathway [24,25]. Farnesoid X receptor (FXR also known as *Nr1h4*) as one kind of BA-activated nuclear receptors is present in both the liver and the small intestine (SI) to regulate the BA homeostasis, include hepatic BA synthesis, intestinal BA absorption, and hepatic BA uptake [22]. Various BA transporters in the enterohepatic circulation are responsible for the entry and exit of these conjugated BAs, such as Na^+-taurocholate cotransporting polypeptide (*Ntcp*), bile-salt export pump (*Bsep*) and apical Na^+-dependent bile-salt transporter (*Asbt*) [26–29]. In addition, the interaction between intestinal microbiota and BAs is not unidirectional but in an active state of communication, and the present study suggests that the association between targeted BAs and intestinal microbiota may provide a surprising new perspective for treatment of cholestatic liver disease.

In this study, a PSC mouse model was established by chemical induction with 3,5-diethoxycarbonyl-1,4-dihydropyridine (DDC) [30–35]. After confirming that the abundance of *P. copri* was significantly reduced in the mouse model, reverse supplementation of *P. copri* was performed, which significantly improved cholestasis in enterohepatic circulation by enhancing the FXR signalling pathway and reducing liver fibrosis in the DDC-induced PSC mice. Thus, *P. copri* was found to have potential application prospects in the treatment of PSC disease, which provides a basis for further research on the treatment of chronic cholestasis diseases with microorganisms.

2. Materials and methods

2.1. P. copri media, culture condition and quantification

P. copri (DSM18205) and blood agar medium were purchased from Mingzhou Biotechnology Co., LTD. The bacteria were incubated in an anaerobic culture tank (volume: 2.5 L, Mitsubishi, Tokyo, Japan) equipped with an anaerobic gas bag to provide an anaerobic environment. Bacterial DNA was extracted using the TIANamp Bacteria DNA Kit (Tiangen Biotechnology Co., LTD.). qPCR was carried out on QuantStudio® 5 Real-Time System (Applied Biosystems), and the cycling conditions were as follows: 95 °C for 5 min, 40 cycles at 95 °C for 10 s, 56 °C for 20 s, and 72 °C for 30 s.

2.2. Animal experiments

7-Week-old male C57BL/J mice were purchased from GemPharmatech Co., LTD., housed with a 12-h light/dark cycle, with no restrictions on their food or water under conditions of controlled humidity (50% ± 5%) and temperature (22 ± 2 °C). All the experimental programs for mice have been approved by the Nanjing Medical University Institutional Animal Care and Use Committee (Approval No. IACUC-2005013). A total of 36 mice were randomly divided into 6 groups with 6 mice in each group for experimental treatment, which were generally divided into two experimental schemes. Two groups were sacrificed to observe the disease effect after 1 week of DDC treatment, and the other four groups were given *P. copri* late intervention. Specific grouping and treatment are as follows: One was Control group and DDC group, with six mice in each group to construct PSC mouse model by feeding 0.1% (w/w) DDC (CAS: 632–93-9; Sigma-Aldrich Co., LTD.) supplemented diet (Synthesized by Jiangsu Xietong Pharmaceutical Bioengineering Co., LTD.) for 1 week. Second, four groups, Control, *P. copri*, DDC and DDC + *P. copri*, with six mice in each group. Mice in Control and *P. copri* group were both fed normal diet all the time, then Control mice were given sterile phosphate buffer solution (1 × PBS; 0.01 M, pH 7.2–7.4) and *P. copri* group mice daily gavage 1×10^8 CFU *P. copri* after one week; Mice in DDC and DDC + *P. copri* group were fed a customized diet all the time for two weeks and fed 0.1% DDC diet for the previous week to construct the model. Then, both groups were given PBS/*P. copri* gavage for one week. *P. copri* was dissolved into bacterial suspension with sterile PBS. OD_{600nm} value were used for concentration conversion based on previous study [36]. Weight was recorded daily from the first day of the experiment. Fresh faces were collected and all the mice were sacrificed after 12 h of starvation at the last day. The collected blood was placed overnight at 4 °C and centrifuged to collect serum. The liver and intestine were excised immediately and then divided, sections were fixed and sliced for further histological and immunohistochemical analysis, the rest was stored at −80 °C until use.

2.3. Magnetic resonance imaging (MRI)

High-field MRI of mice was performed on a Biospec 70/20 USR instrument (Bruker, BioSpin, Ettlingen, Germany). Mice were anesthetized with isoflurane during imaging (~2% in 67% air and 33% O_2), and isoflurane levels were adjusted as needed to maintain a breathing rate of about 60 breaths/min. The rapid acquisition with relaxation enhancement sequence (RARE) was used to collect the photos, and the echo time (TE) = 33.0 ms and time of repetition (TR) = 3089.6 ms.

2.4. Biochemical parameters analysis of serum

Serum biochemical indexes including aspartate aminotransferase (AST), alanine aminotransferase (ALT), alkaline phosphatase (ALP), and total bilirubin (TBI) in serum were detected by automatic biochemical analyser (Hitachi 7100).

2.5. Measurement of TBAs in serum and liver and intestine

The levels of total BAs (TBAs) in serum, liver and SI were detected using TBAs kits (No. E003–2-1; Jiancheng Bioengineering Institute) according to the manufacturer's protocol.

2.6. Measurement of hydroxyproline in serum and liver

Hydroxyproline in serum and liver of mice in each group was detected using hydroxyproline assay kit (No. A030–2-1; Jiancheng Bioengineering Institute) according to the manufacturer's protocol.

2.7. 16S rRNA sequencing

Microbial DNA from faecal samples of mice ($n = 6$) was extracted for 16S rRNA sequencing on an Illumina MiSeq platform (Illumina, San Diego, USA). The taxonomy of each 16S rRNA gene sequence was analysed by RDP Classifier algorithm (http://rdp.cme.msu.edu/) against the Silva 138/16S rRNA database using confidence threshold of 70%. The data is stored and analysed on the I-Sanger Bio-cloud platform by Shanghai Majorbio Bio-pharm Technology Co. Ltd. The student's *t*-test was used to obtain alpha diversity Sobs, Shannon and Ace indexes. Abund_jaccard test was performed to evaluate each grouping condition at OTU level in PCoA (principal coordinate analysis). Kruskal-Wallis rank sum test, FDR multiple test correction, and Tukey-Kramer post hoc test (giving a 95% confidence interval for the mean) were used to detect differences in the abundance of bacterial genera in the four treatment groups. A two-matrix correlation heat map was used to analyse the bacterial genus abundance data and BAs content data, and the correlation coefficient was Spearman.

2.8. Targeted determination of BAs using LC/MS

The types and contents of BAs in stool samples were analysed by liquid chromatography-mass spectrometry (LC-MS). A total of 46 BAs were available for analysis (Table S1). Various BAs in faecal samples were qualitatively and quantitatively detected by LC-ESI-MS/MS analysis method. In the process, the mixed standard liquid was firstly

prepared, 46 kinds of standard substances were weighed, methanol was added at constant volume, and then the reserve liquid was obtained after eddy mixing. Add 50% methanol and dilute it to the working solution, then accurately weigh 50 mg sample and add 400 μL extract (methanol: water = 4:1), grind it for 6 min (−10 °C, 50 Hz) in the frozen tissue grinding machine, ultrasonic for 30 min (5 °C, 40 kHz) in the low temperature ultrasonic machine, stand it for 30 min at −20 °C, centrifuge for 15 min (4 °C, 13000 g), take 200 μL supernatant and test it on the machine.

2.9. Histopathology

The liver and intestinal tissues were fixed with 4% paraformaldehyde for more than 24 h. Tissues from each mouse were then paraffin embedded, cut into 4 μm thick and stained with haematoxylin and eosin (H&E), Sirius red (SR) and immunohistochemical (IHC). IHC staining was used to analyse the extent of immune cell infiltration (F4/80 [37] and CD11b [38,39]), bile duct epithelial cell proliferation (CK19), and liver fibrosis (αSMA). According to standard procedures, the main experimental steps included fixing, paraffinizing, deparaffinizing, dehydrating, antigen retrieval, blocking endogenous peroxidase activity, sealing, primary antibody incubation, washing, sealing, secondary antibody incubation, washing, chromogenic, nucleus counterstaining, dehydration and mounting, and observation. Pannoramic scanning (3DHISTECH, Hungary) was used to obtain representative images by blind scanning the stained slides. ImageJ software was used for all quantitative analyses.

2.10. RNA extraction and quantitative real-time PCR

Total RNA was extracted using the FastPure Cell/Tissue Total RNA Isolation Kit (Cat: RC101–01; Vazyme, Biotech) and reverse transcribed into cDNA using the HiScript II Q RT SuperMix (Cat: R223–01; Vazyme, Biotech). The concentration and purity of total RNA was detected using NanoDrop2000 spectrophotometer (NanoDrop Technologies; Thermo Fisher Scientific, Inc.). Then real-time PCR was used to quantitatively detect the corresponding gene expression. Enriched cDNA, forward primer, reverse primer (0.2 μM, respectively, see Table S2 of oligonucleotides sequences; synthesized by Genscript Biotech Corporation, Nanjing, China), Hieff® qPCR SYBR® Green Master Mix (5 μL, Cat: 11202ES08, Yeasen Biotech Co., LTD.) were mixed up to 10 μL volume. The mixture was subject to qPCR on AB RT-PCR (Q5). RT-qPCR analysis was performed in triplicate. *Gapdh* was used as the internal control for the expression level of target genes, and the relative expression level was evaluated using $2^{-\Delta\Delta Ct}$ method.

2.11. Protein extraction and Western blot analysis

Total proteins in liver and SI tissue samples were extracted using RIPA lysis buffer (Beyotime Biotechnology, Shanghai, China) with protease inhibitor and homogenized using Tissue Lyser II (Dusseldorf, Germany). The protein concentrations in the supernatant fluid were then determined using Pierce BCA protein assay reagent (Beyotime Biotechnology, Shanghai, China). After boiling with 1× loading buffer, the proteins were separated by electrophoresis on 12% SDS-PAGE gels and subsequently transferred to polyvinylidene fluoride (PVDF) membranes (Millipore, Billerica, MA, USA). A solution, containing 3% BSA-TBST, was applied to block the membranes for 30 min at room temperature (25 °C). Then, the membrane was incubated overnight at 4 °C with the following primary antibodies: (a) rabbit anti-FGF15 (1:2000, Abcam, ab229630); (b) mouse anti-GAPDH (1:10000, Immunoway, YM3029). Afterwards, the membranes were incubated with secondary antibodies for 2 h at room temperature, then the bands were visualized with Chemiluminescent HRP Substrate (Millipore Corporation, Billerica, MA, USA). All experiments were repeated at least three times. The results were normalized to the counterparts of GAPDH and analysed with ImageJ software (NIH, Bethesda, MD, USA).

2.12. Statistical analysis

Diagrams and data in this study were expressed as mean ± standard error of mean (SEM). For two-group comparison, unpaired two-tailed Student's *t*-test was used. For comparison of the four treatment groups, one-way analysis of variance (ANOVA) followed by LSD multiple comparison test was used. Data were analysed using GraphPad Prism 8 (GraphPad Software Inc., USA). Special and specific analysis was presented in the legend of each corresponding chart. $p < 0.05$ was considered statistically significant.

3. Results

3.1. The DDC diet induced a PSC model in mice and significantly decreased P. copri abundance

Mice were fed a diet supplemented with 0.1% (w/w) DDC for one week, and their body weight was significantly reduced from the 3rd day compared with that of Control mice (Fig. 1A). MRI cholangiography and serum biochemical tests revealed that DDC diet-fed mice exhibited a beadlike obstruction in the intrahepatic bile ducts (Fig. 1B) and significantly increased serum ALP, ALT, AST and TBI levels (Fig. 1C), suggesting that the DDC diet could induce symptoms and pathological changes in mice similar to those in sclerosing cholangitis, accompanied by serious damage to liver function. In addition, an increased serum level of the bile component TBI suggested the occurrence of cholestasis in the DDC group. Furthermore, the levels of TBAs in the serum and liver were upregulated, while the levels of TBAs in the small intestine (SI) were significantly deficient (Fig. 1D). This result indicated that severe cholestasis in the serum and liver was present in the DDC group and that the TBA pool in the SI was inadequate. Moreover, based on liver and colon (Fig. S1A) pathology, DDC-fed mice displayed evident inflammatory cell aggregation (Fig. 1E). In order to observe the aggregation of inflammatory cells in liver tissue intuitively, we detected two cell markers of macrophages, F4/80 and CD11b, through immunohistochemistry, and the results showed that the number of peri-duct macrophages and liver-specific macrophages in mice of the DDC group was significantly increased (Fig. 1E). In quantitative terms, the number of macrophages and Kupffer cells in the liver of mice in DDC group was nearly four and eight times that of the control group, respectively (Fig. 1G). On the other hand, based on IHC analysis, the bile duct epithelial marker CK19 was highly expressed in the livers of mice in the DDC group (Fig. 1F), and its expression was significantly increased by more than sevenfold compared with that in the control group (Fig. 1G), suggesting that DDC induced obvious ductal reactions and cholestasis. Additionally, DDC-fed mice developed sclerotic cholangitis and severe intrahepatic periductal fibrosis with characteristic onion-like fibrosis, as determined by SR staining and αSMA IHC (Fig. 1F). Analysis of IHC staining area showed that the positive expression of αSMA in the DDC group was approximately 17 times higher than that in the control group (Fig. 1G). Considering that an intestinal microbiota analysis of PSC patients showed a significant reduction in *P. copri* compared with healthy people [11], we next tested the abundance of *P. copri* in the faeces of model mice using qPCR. The results showed that *P. copri* abundance was significantly inhibited in the intestines of mice in the DDC group, which was consistent with the report in patients with PSC (Fig. 1H). Taken together, these findings suggest that a diet supplemented with 0.1% (w/w) DDC can induce a primary sclerosing cholangitis model in mice and significantly decrease the abundance of *P. copri*.

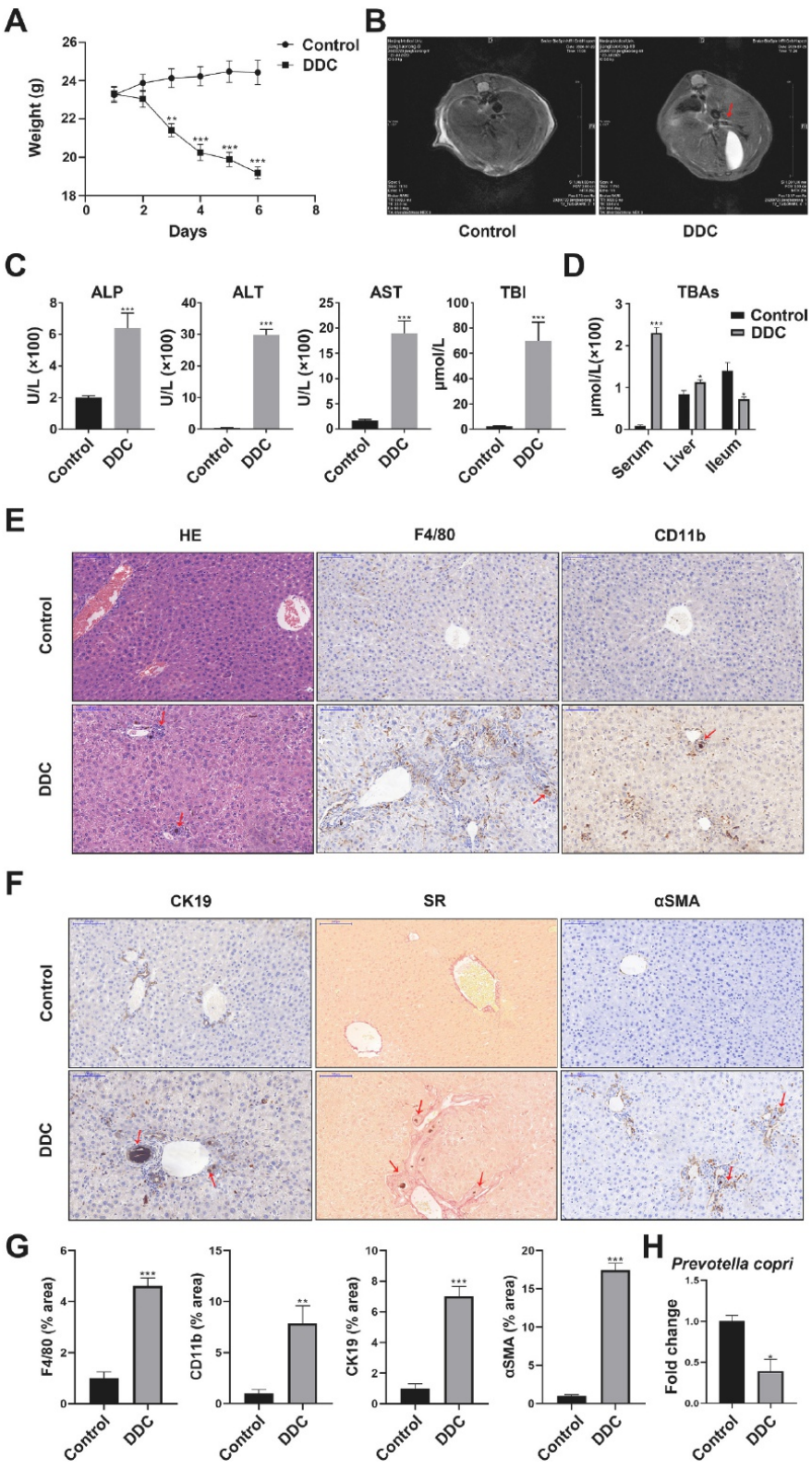

Fig. 1. PSC mouse model was successfully induced by feeding 0.1% (w/w) DDC to healthy mice for 1 week. (A) Daily body weight of mice in the control group ($n = 6$) and DDC group ($n = 6$). (B) Mice from the Control group and the DDC group for MRI biliary duct imaging, and two representative images were found for observation. Obviously beaded biliary duct obstruction was observed in intrahepatic bile ducts, as indicated by the red arrow. (C) The serum ALP, ALT, AST and TBI concentrations of each mouse were detected using serum biochemical tests. (D) Determination of TBAs in the serum, liver and SI. Each sample was tested three times in parallel. (E) After H&E staining of liver sections, inflammatory cell aggregation and bile duct cholestasis (marked by a red arrow) were observed in the model group induced by DDC, and obvious positive areas (shown with a red arrow) were observed in the DDC group after IHC staining of F4/80, CD11b, (F) CK19 (cytokeratin 19) and αSMA (α smooth muscle actin). For the quantification of staining positive areas, 6 visual fields were randomly selected for each section, and area statistics were carried out by IHC tool of ImageJ software. Regional area analysis was performed in (G). (F) SR staining revealed characteristic onion-like fibrosis around the bile ducts. (H) Faecal samples of each group were divided into three parallel samples, and the abundance of *Prevotella copri* and the bacterial universal primer was analysed by qPCR. Scale bar 100 μm; original magnification 20×; $^{*}p < 0.05$, $^{**}p < 0.01$, $^{***}p < 0.001$, difference was analysed by unpaired two-tailed Student's *t*-test.; $n = 6$.

3.2. P. copri intervention had no effect on body weight or the inflammatory response in mice but improved liver function impairment and fibrosis

The experimental design is shown in Fig. 2A. Before the animal experiment, *P. copri* was observed by Gram staining with oil microscope (Fig. S2A), and the PCR product was identified by agarose gel electrophoresis with specific primers (Fig. S2B). The results confirmed that *P. copri* was a Gram-negative bacterium. After gavage, the abundance of *P. copri* in the intestine was significantly increased compared with that in the control group, while *P. copri* intervention effectively offset the reduction caused by DDC to a level close to the content in the control group (Fig. 2B). Oral inoculation of *P. copri* failed to recover DDC diet-induced body weight loss in the DDC + *P. copri* group compared

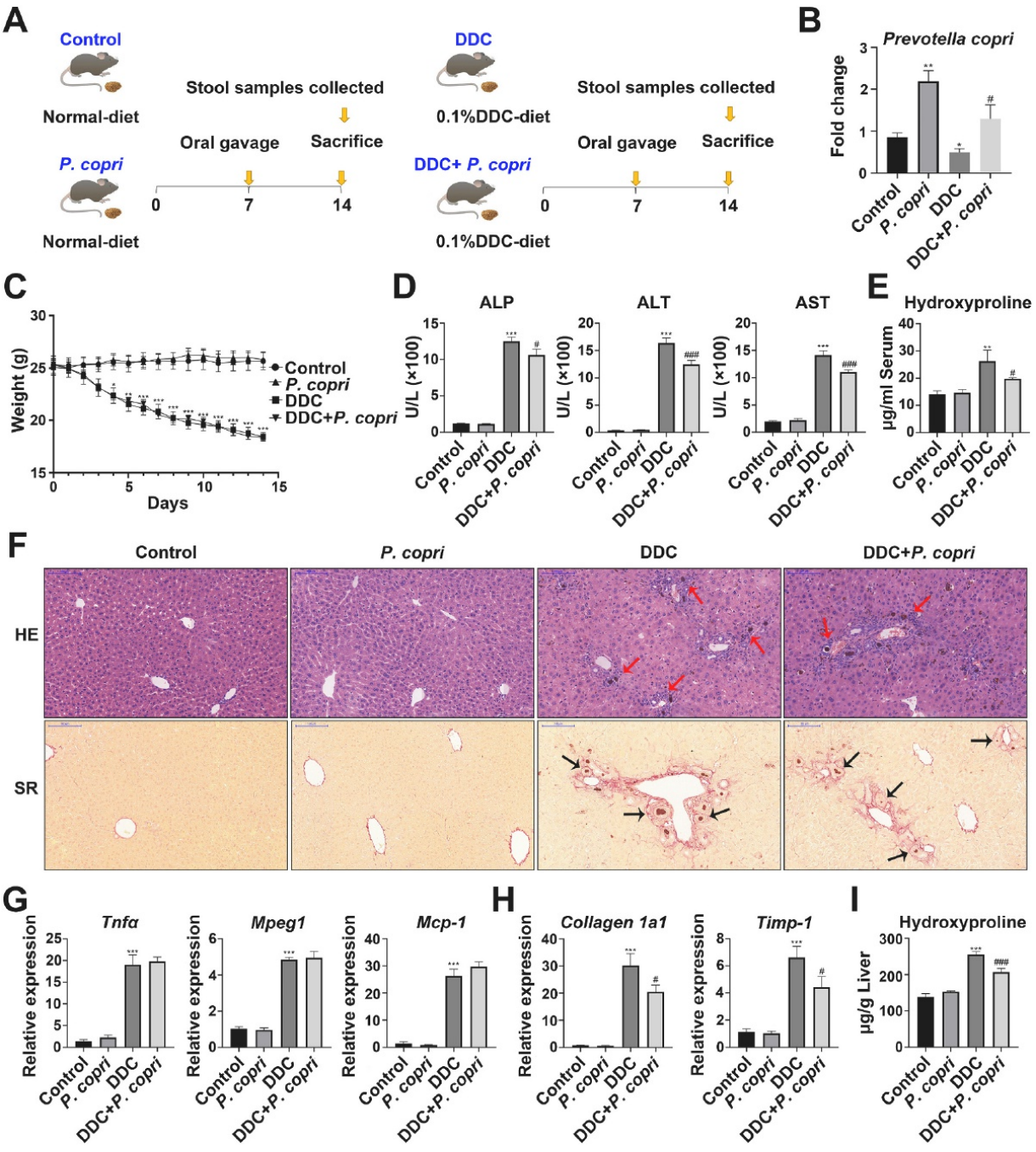

Fig. 2. Mice in Control group and *Prevotella copri* group were fed normal diet for two weeks, and mice in DDC group and DDC + *P. copri* group were fed 0.1% (w/w) DDC added diet for two weeks. In the second week, mice in *P. copri* group and DDC + *P. copri* group were given 1×10^8 CFU *P. copri* orally. The other two groups were given equal volume of PBS orally. Changes in various sclerosing cholangitis phenotypes in mice after *P. copri* intervention. (A) Schematic diagram of treatment measures for four groups of mice. (B) Faecal samples of each group were divided into three parallel samples, and the abundance of *P. copri* in the intestines of the four groups of mice was measured by qPCR. Universal 16S Primers serves as a reference for expression. (C) The daily weight changes of mice in each group after four treatments. (D) Serum ALP, ALT and AST concentrations were measured by automatic biochemical analysis. (E) Serum hydroxyproline content of mice in four groups. (F) Pathological phenotype of livers observed after H&E and SR staining. Red arrows indicate inflammation, and black arrows indicate fibrotic phenotypes. (G) The transcripts of *Tnfα*, *Mpeg1*, *Mcp-1*, (H) *Collagen 1a1* and *Timp-1* in the liver. Each gene expression was measured three times in parallel. (I) Liver hydroxyproline levels of mice in each group. Values were determined for three parallel samples per group for each sample. Scale bar 100 μm; original magnification 20×; * indicates statistical differences in the *P. copri* group and DDC group compared with the Control group, and # indicates the statistical difference between the DDC + *P. copri* group and the DDC group; $^*p < 0.05$, $^{**}p < 0.01$, $^{***}p < 0.001$; $\#p < 0.05$, $\#\#p < 0.01$, $\#\#\#p < 0.001$, difference was analysed by one-way analysis of variance (ANOVA) followed by LSD multiple comparison test; $n = 6$.

with the DDC group, and separate administration of *P. copri* did not affect the body weight of mice compared to mouse weights in the control group (Fig. 2C). However, DDC + *P. copri* treatment significantly decreased the serum biochemical indexes of ALP, ALT and AST compared to those in the DDC group, but the indexes did not recover to the normal levels observed in the control group (Fig. 2D). This indicates that *P. copri* treatment in a DDC background can partially recover and reduce liver injury in a PSC model. Additionally, based on H&E and SR staining, accumulation of inflammatory cells around the bile ducts and onion-like fibrosis were obviously present in both the DDC group and DDC + *P. copri* group, suggesting that *P. copri* intervention after DDC treatment did not completely restore the liver inflammation and fibrosis induced by DDC (Fig. 2E). The mRNA expression levels of the inflammatory factors *Tnfα*, *Mpeg1* and *Mcp-1* in liver tissue were further detected by qPCR (Fig. 2F). Consistent with the pathological results, the levels of inflammatory cytokines in the *P. copri* group were approximately the same as those in the control group, while the expression levels of *Tnfα*, *Mpeg1* and *Mcp-1* in the DDC group and the DDC + *P. copri* group were increased, indicating that *P. copri* intervention did not improve inflammation. However, the expression of the fibrosis indicator factors *Collagen 1a1* and *Timp-1* in liver tissue were significantly reduced in the liver tissue of model mice after DDC intervention with *P. copri* (Fig. 2G), indicating that *P. copri* treatment can improve the liver fibrosis progression caused by DDC. In addition, since hydroxyproline is a specific amino acid in collagen and is used as a marker for evaluating fibrosis in vivo [40–42], we measured its levels in serum and liver of four groups of mice (Fig. 2E and I). The results showed that the concentration of hydroxyproline increased after DDC treatment, but decreased significantly after the addition of *P. copri*. It was further indicated that *P. copri* had a significant improvement effect on fibrosis.

3.3. Intervention with *P. copri* significantly improved cholestasis in enterohepatic circulation caused by the DDC diet and affected the composition of conjugated and unconjugated BAs

After DDC treatment, the addition of *P. copri* reduced the level of TBI in the serum of mice, suggesting that *P. copri* treatment can improve DDC diet-induced cholestasis (Fig. 3A). The content of TBAs in enterohepatic

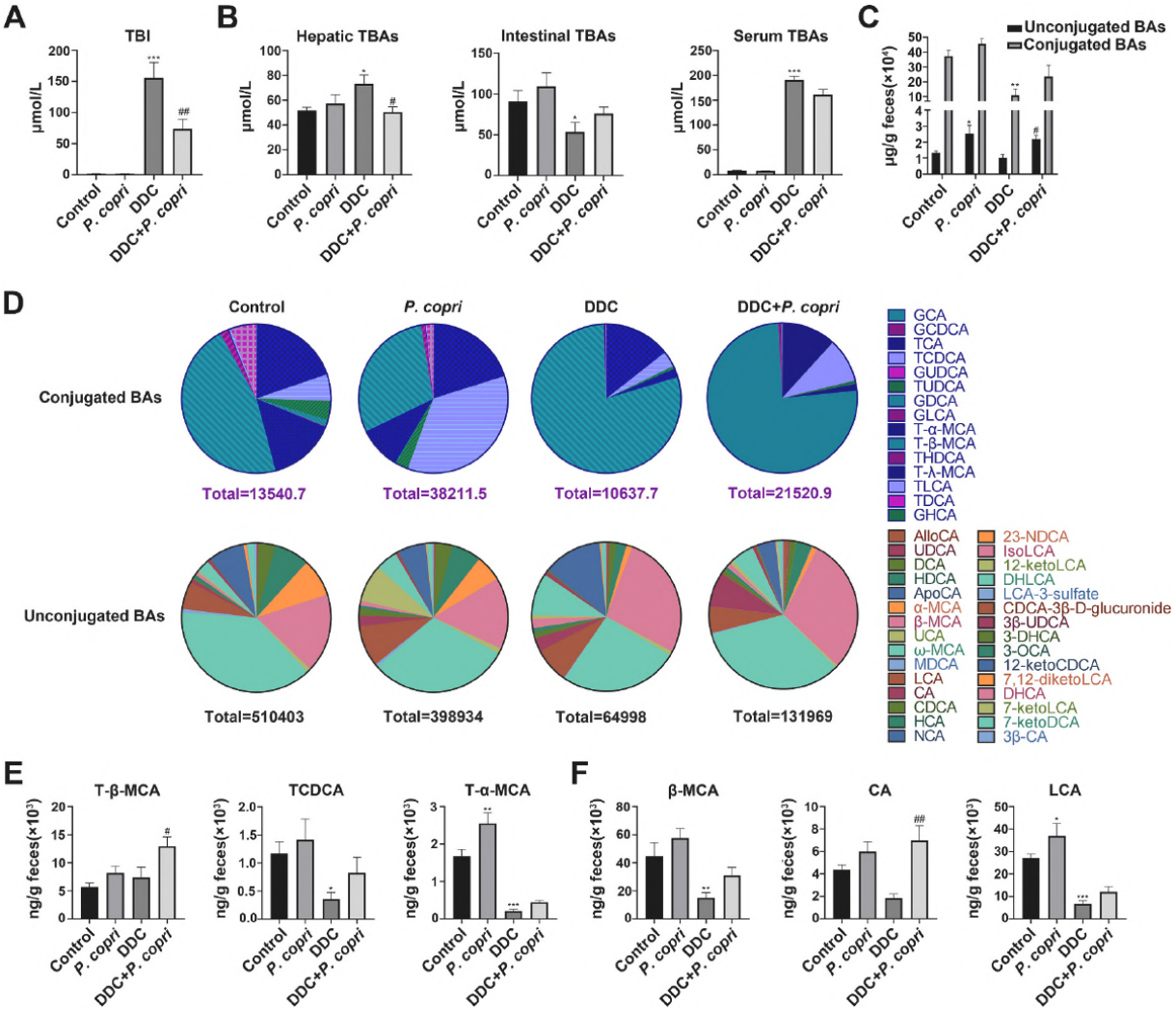

Fig. 3. The changes of TBI, TBA and specific BAs in serum and tissues of mice in four groups were detected. In general, *Prevotella copri* intervention after DDC treatment significantly improved BA metabolism. (A) Serum TBI content of mice in four groups. (B) The concentrations of TBAs in serum and supernatant of liver and SI of mice in the four experimental groups. Values were determined for three parallel samples per group for each sample. (C) By classifying the structures of 46 BAs detected, they were divided into conjugated and unconjugated BAs. The conjugated BAs were all conjugated with glycine or taurine, and the rest were unconjugated BAs. Accordingly, the contents of these two BAs in the faeces of mice in four different treatment groups were analysed via targeted quantitative analysis of BAs. (D) The specific proportions of BAs among the two types of BAs are shown in the pie chart, and the top three BAs with varying degrees and proportions were screened out, as shown in (E) and (F). * indicates statistical differences in the *P. copri* group and DDC group compared with the control group, and # indicates the statistical difference between the DDC + *P. copri* group and the DDC group; $^{*}p < 0.05$, $^{**}p < 0.01$, $^{***}p < 0.001$; $\#p < 0.05$, $\#\#p < 0.01$, $\#\#\#p < 0.001$; $n = 6$.

circulation was also balanced and improved in the DDC + *P. copri* group. This was demonstrated by the reduction of TBA levels in the liver to normal levels and restoration of the deficiency in TBA pools in the SI to the level in the control group (Fig. 3B). Meanwhile, the TBA levels in the liver, SI and serum in the *P. copri* group were not significantly different from those in the control group (Fig. 3B). Therefore, these data demonstrate that intervention with *P. copri* under a DDC background realized recovery of the TBA levels in the liver and SI, while the TBAs were still heavily deposited in the serum. To explore specific changes in the BA composition, forty-six targeted BAs were further assessed via quantitative analysis. A total of 46 BAs were detected, and all the unclassified BAs were analysed to observe the proportion and content of various BAs in each group of mice (Fig. S3A). Since intestinal microbiota plays a key role in the transformation of BAs, we further refined BAs into conjugated and unconjugated BAs. Compared with the control group and the DDC group, the content of both types of BAs tended to increase in the two *P. copri* intervention groups (Fig. 3C). The proportions of specific BAs among the two BA types in each group are presented in pie charts in Fig. 3D. By comparing the four treatment groups, T-β-MCA (57.61% ± 0.2067), TCDCA (13.50% ± 0.1285) and T-α-MCA (6.84% ± 0.05451) were found to be the top three conjugated BAs with the highest proportion and the widest range of variation among the four groups (Fig. 3E). In addition to these three types of conjugated BAs, quantitative analysis data can be seen in Fig. S3B. Although both T-β-MCA and T-α-MCA have been identified as natural FXR antagonists [43], our results showed that the T-β-MCA content was significantly increased only in the DDC + *P. copri* group, but T-α-MCA expression was increased after *P. copri* intervention compared with the level in the control group and recovered from the reduced level caused by DDC. In addition, TCDCA has been reported to bind to human TGR5, thereby regulating TGR5 activity [44]. The content of TCDCA in the *P. copri* group was increased compared with that in the DDC group, and after the addition of *P. copri*, the level of TCDCA in the DDC group was restored to the level observed in the control group. A similar screening was performed for unconjugated BAs, focusing on β-MCA (22.38% ± 0.06064), CA (3.41% ± 0.02588), and LCA (7.13% ± 0.01298) (Fig. 3F). Among them, CA and LCA are effective endogenous ligands of FXR [45,46]. In addition to these three, the remaining unconjugated BAs detected by quantitative analysis can be seen in Fig. S3C. Collectively, these results suggest that *P. copri* treatment may stimulate the receptors of BAs and activate the relevant signalling pathways to alleviate cholestasis induced by the DDC diet and affect the composition of conjugated and unconjugated BAs.

3.4. FXR-related pathways were distinctly activated after *P. copri* inoculation to regulate BA synthesis and transport in enterohepatic circulation

To further address how *P. copri* treatment improve DDC-induced cholestasis, qPCR was performed to detect the expression of seven specific BA receptors in liver tissue (Fig. 4A). Both *Fxr* and *Rorγ* were significantly increased after *P. copri* administration in control and DDC mice. In addition, compared with the DDC group, *Fxr*, *Lxrα*, *Rorα* and *Rorγ* were increased in the *P. copri* group, while *Fxr*, *Lxrβ*, *Tgr5* and *Rorα* were increased in the DDC + *P. copri* group. These data further suggest that *P. copri* intervention generally stimulated these BA receptors to synergistically maintain BA homeostasis in the liver. Obviously, *Fxr* was the only one receptor in liver tissues increased in *P. copri* group and distinctly inhibited in DDC group, indicating that the negative feedback regulation mechanism of FXR in BA production was alleviated, leading to the occurrence of DDC-induced cholestasis. As evidenced of significantly up-expressed nuclear receptor *Shp*, a target gene of *Fxr* that represses LRH-1 [45], in liver of mice in *P. copri* group but significantly inhibited in DDC group (Fig. 4C), lead to significantly elevated transcription of *Cyp7a1* in the liver in DDC group (Fig. 4B). Consistent with our findings, DDC induced cholestasis by significantly increasing *Cyp7a1*

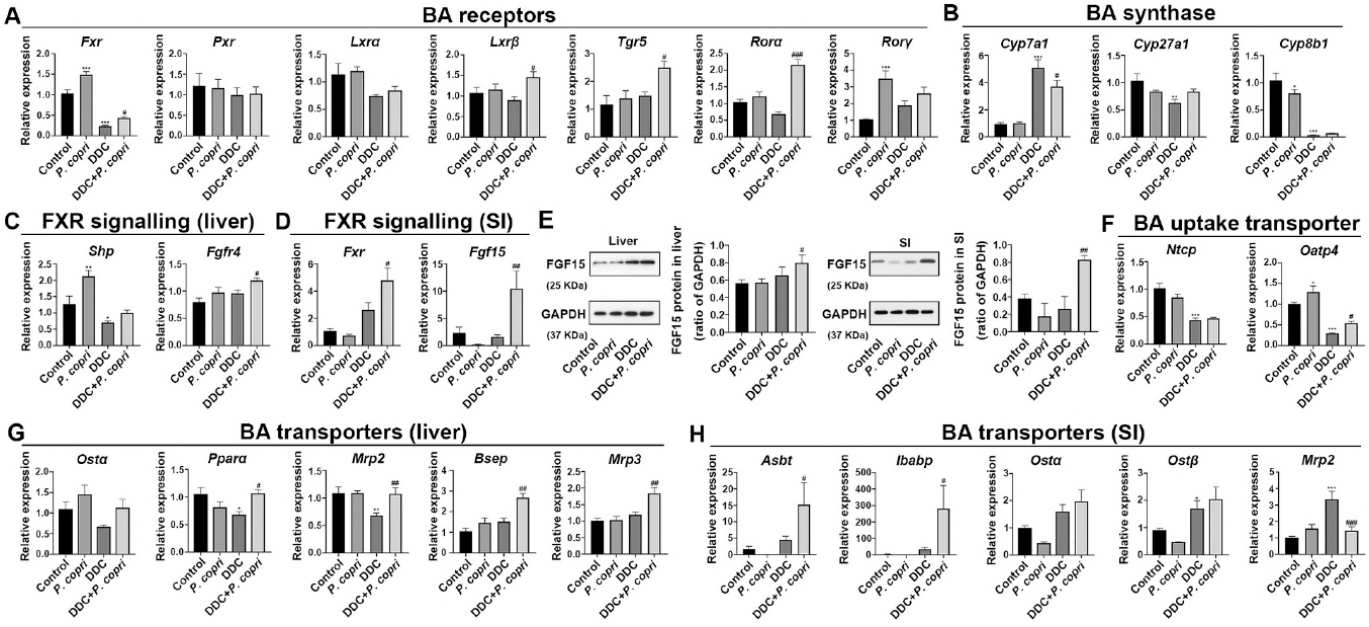

Fig. 4. Expression and secretion of BA receptor and synthase in liver (A/B) and expression of FXR signalling pathway genes and BA transporter in liver and SI (C—H) of mice in four groups. *Gapdh* was used as the internal control. Gene expression results were measured three times in parallel for each group of mice and protein assays were measured three times in parallel for each group of three mice. (A) Comparison of the levels of seven BA receptors (*Fxr*, *Pxr*, *Lxrα*, *Lxrβ*, *Tgr5*, *Rorα*, *Rorγ*) in the liver of each group. (B) Levels of BA synthase in the BA synthesis pathway in the liver. Changes in the expression levels of various signalling molecules involved in the *Fxr-Cyp7a1* negative feedback signalling pathway in the (C) liver and (D) SI. (E) Western blotting was used to determine the relative expression level of FGF15 compared with GAPDH protein in liver ($n = 3$) and SI ($n = 3$). (F) Expression of *Ntcp* and *Oatp4* in the liver. (G) Levels of genes in the BA transport system regulated by *Fxr* directly or indirectly through *Pparα* in the liver. (H) Changes in BA receptors and *Fxr*-regulated BA transporters in the SI after four treatments. (* indicates statistical differences in the *Prevotella copri* group and DDC group compared with the control group, and # indicates the statistical difference between the DDC + *P. copri* group and the DDC group; $*p < 0.05$, $**p < 0.01$, $***p < 0.001$; $\#p < 0.05$, $\#\#p < 0.01$, $\#\#\#p < 0.001$); $n = 3$–6.

(Fig. 4B). Meanwhile, *Cyp27a1* was decreased after DDC induction, indicating that BA synthesis in the model group was mainly realized through the classical pathway. In addition, *Cyp8b1* was decreased in all three groups except the control group, consistent with the results of targeted BA detection, further explaining why CDCA synthesis was more common than CA in the DDC + *P. copri* group (Fig. S3D). Above results indicate that *P. copri* can rescue DDC-induced cholestasis by reducing BA synthesis through the *Fxr-Cyp7a1* pathway in the liver. However, the level of *Shp* in the DDC + *P. copri* group was consistent with that in the control group; thus, we speculated that *P. copri* intervention increased *Fxr* to activate *Shp* via negative feedback that inhibited the elevation of DDC-induced *Cyp7a1* in the DDC + *P. copri* group. On the other hand, after DDC treatment, although *Fxr* in the SI showed no significant difference compared with that in the control group (Fig. 4D), *Fxr* was significantly expressed in the DDC + *P. copri* group; thus, a large amount of *Fgf15* was recruited and received through the circulatory system to bind *Fgfr4* on the liver surface to negatively inhibit *Cyp7a1* through *Fgfr4* (Fig. 4C and D). In addition, western blot was used to detect FGF15 protein expression levels in liver and SI tissues of the four groups of mice as shown in Fig. 4E. The results showed that compared with DDC group, the expression of FGF15 protein in liver and SI of DDC + *P. copri* group was increased by 1.24 ± 0.13 and 26.88 ± 42.87 fold respectively. Therefore, above results further demonstrated that FXR signalling pathway was activated in DDC + *P. copri* group. However, from the perspective of regulation of the BA synthesis pathway, the *Fxr-Cyp7a1* signalling pathway in the liver did not recover to the same level as that in the control group after DDC plus *P. copri* intervention, which was inconsistent with the change in liver TBAs.

The gene expression of BAs-related transporters in the liver (Fig. 4F and G) and SI (Fig. 4H) was detected via qPCR. First, the expression of uptake transporter for BAs *Ntcp* and *Oatp4* were decreased in DDC mice. And DDC + *P. copri* treatment upregulated *Oatp4* compared to that in the DDC group, indicating that activation of *Fxr* correspondingly increased *Oatp4* expression in the DDC + *P. copri* group (Fig. 4F). In addition, *Fxr* simultaneously regulated *Pparα*, resulting in *Ostα*, *Mrp2*, *Bsep*, and *Mrp3* responses (Fig. 4G). These transporters work together to transfer BAs through the bile duct system to the SI. After BAs travel through the biliary tract system to the SI, *Ostβ* and *Mrp2* were increased in the DDC group (Fig. 4H). This indicates that a large number of BAs in the SI of mice in the DDC group were transferred out and lost through systemic circulation, resulting in deficiency of the TBA pool in the SI. However, the expression of *Asbt* and *Ibabp* in the DDC + *P. copri* group was higher than that in the DDC group, which was probably caused by activation of intestinal *Fxr* (Fig. 4D). Meanwhile, the expression of *Ostα* and *Ostβ* increased in the SI (Fig. 4H). The expression levels of *Ostα* and *Ostβ* in the DDC + *P. copri* group were approximately twice as high as those in the control group, while the level of *Ibabp* was more than 300-fold as high as that in the control group. The increase in *Ostα* and *Ostβ* was much lower than the increase in *Ibabp*, which results in a large number of BAs being accepted by *Asbt* and binding with *Ibabp* and therefore remaining in the SI, thus playing a role in balancing the TBA pool in the SI.

In summary, we reveal the mechanism by which *P. copri* improves and restored BA distribution and metabolism in enterohepatic circulation from two aspects. The first aspect is the overall mobilization of the *Fxr-Cyp7a1* signalling pathway. When *P. copri* was applied to DDC mice, the response of *Fxr* in liver and SI was significantly enhanced. *Fxr* in the liver activates *Shp*, and together with *Fgf15* receptor *Fgfr4*, which is stimulated by *Fxr* in the SI, promotes *Cyp7a1* inhibition and reduces BA synthesis. Intrahepatic *Fxr* stimulation of *Pparα*, on the other hand, increases the expression of multiple BA excretion proteins, while intestinal *Fxr* aggregates more *Ibabp* to receive increased absorption of BAs with *Asbt* to compensate for intestinal BA deficiency. And ultimately balance the BA in the enterohepatic circulation.

3.5. Changes in the faecal microbiome associated with P. copri intervention in mice in different treatment groups and correlation analyses between different bacterial genera and BAs

The gut microbiota is known to play an important role in BA biotransformation in enterohepatic circulation. 16S rRNA sequencing to assess intestinal microbial diversity revealed that single-species bacterial intervention with *P. copri* may have a great impact on the overall intestinal microbiota (Fig. 5A). Species of intestinal microbiota in the DDC + *P. copri* group was significantly richer than in the control group and/or DDC group, which was reflected by a higher Sobs index and Ace index (Fig. 5A). Additionally, the Shannon index indicated that *P. copri* administration in the DDC + *P. copri* group increased the diversity of the gut microbiota in comparison with that in the DDC group, but not of the control group (Fig. 5A). Furthermore, the intestinal microbiota composition in the four treatment groups was indeed distinct, which was verified by PCoA and supervised PLS-DA analysis (Fig. 5B). In addition, a Venn chart showed the common and unique OTUs among each group, which provided a basis for our subsequent detection of different bacterial genera (Fig. 5B). As shown in the Venn diagram, there were 12, 19, 11 and 20 characteristic OTUs in the control group, the *P. copri* group, the DDC group and the DDC + *P. copri* group, respectively, and a total of 427 identical OTUs in the four groups. Therefore, *P. copri* administration increased the diversity and richness of the intestinal microbiota compared to the control group, and there were marked differences among the four groups in common and specific bacterial genera. In the analysis of differential microbiota, the top 15 bacterial genera in the abundance list for the four groups were prioritized (Fig. 5C), but the change trends were different; for example, the content of *norank_f_Muribaculaceae* increased significantly after *P. copri* intervention but was inhibited after DDC treatment. There were also bacterial genera, such as *Staphylococcus*, that proliferated rapidly in the DDC group but were decreased in the DDC + *P. copri* group. Interestingly, *Prevotellaceae* were not found among the top 15. Therefore, we speculated that *P. copri* worked together with other bacteria to improve cholestasis in model mice by changing the microenvironment of the intestinal microbiota. As shown in Fig. 5D, the abundance of *norank_f_Muribaculaceae*, *Lactobacillus*, *Turicibacter*, *Bifidobacterium*, *Clostridium_sensu_stricto_1*, *Odoribacter and Alistipes* decreased in the DDC group but recovered in the DDC + *P. copri* group. Conversely, the abundance of *Staphylococcus* and *Akkermansia* increased significantly in the DDC group but decreased after *P. copri* intervention (Fig. 5E). The above two cases reflect the positive effect of *P. copri* treatment on the balance regulation of intestinal microbiota. As the intestinal microbiota plays an important role in the deconjugation process of BAs, we analysed the correlation between bacterial genera and BAs in the four groups, as shown in Fig. 5F. The contribution of different bacterial genera to the generation of BAs was mainly evaluated through the change in the OTU number of intestinal microbiotas in the different treatment groups, corresponding to the change in the concentration of the six BAs described in Fig. 3. The results showed that *Prevotellaceae_UCG-001* and *Turicibacter* were positively related to the TCDCA ($r = 0.53$, $p = 0.08$; $r = 0.53$, $p = 0.08$, respectively), T-α-MCA ($r = 0.56$, $p = 0.004$; $r = 0.64$, $p = 0.0008$, respectively) and LCA ($r = 0.59$, $p = 0.002$; $r = 0.63$, $p = 0.0009$, respectively) level. T-α-MCA and LCA levels were positively correlated with *norank_f_Muribaculaceae* ($r = 0.62$, $p = 0.001$; $r = 0.68$, $p = 0.0002$, respectively) and negatively correlated with *Staphylococcus* ($r = -0.76$, $p = 0.00001$; $r = -0.72$, $p = 0.00008$, respectively). *Odoribacter* was positively correlated with five BAs ($r = 0.56$, $p = 0.004$; $r = 0.43$, $p = 0.04$; $r = 0.58$, $p = 0.003$; $r = 0.7$, $p = 0.0001$; $r = 0.44$, $p = 0.03$) but not T-α-MCA ($r = 0.37$, $p = 0.07$). *Clostridium_sensu_stricto_1* was positively correlated with four BAs ($r = 0.60$, $p = 0.002$; $r = 0.50$, $p = 0.01$; $r = 0.52$, $p = 0.01$; $r = 0.43$, $p = 0.04$) but not T-β-MCA ($r = 0.38$, $p = 0.07$) or β-MCA ($r = 0.32$, $p = 0.1$). *Alistipes* was positively correlated with T-β-MCA ($r = 0.42$, $p = 0.04$) and CA ($r = 0.52$, $p = 0.01$). *Akkermansia* was negatively correlated with T-α-MCA, β-MCA and LCA ($r = -0.57$,

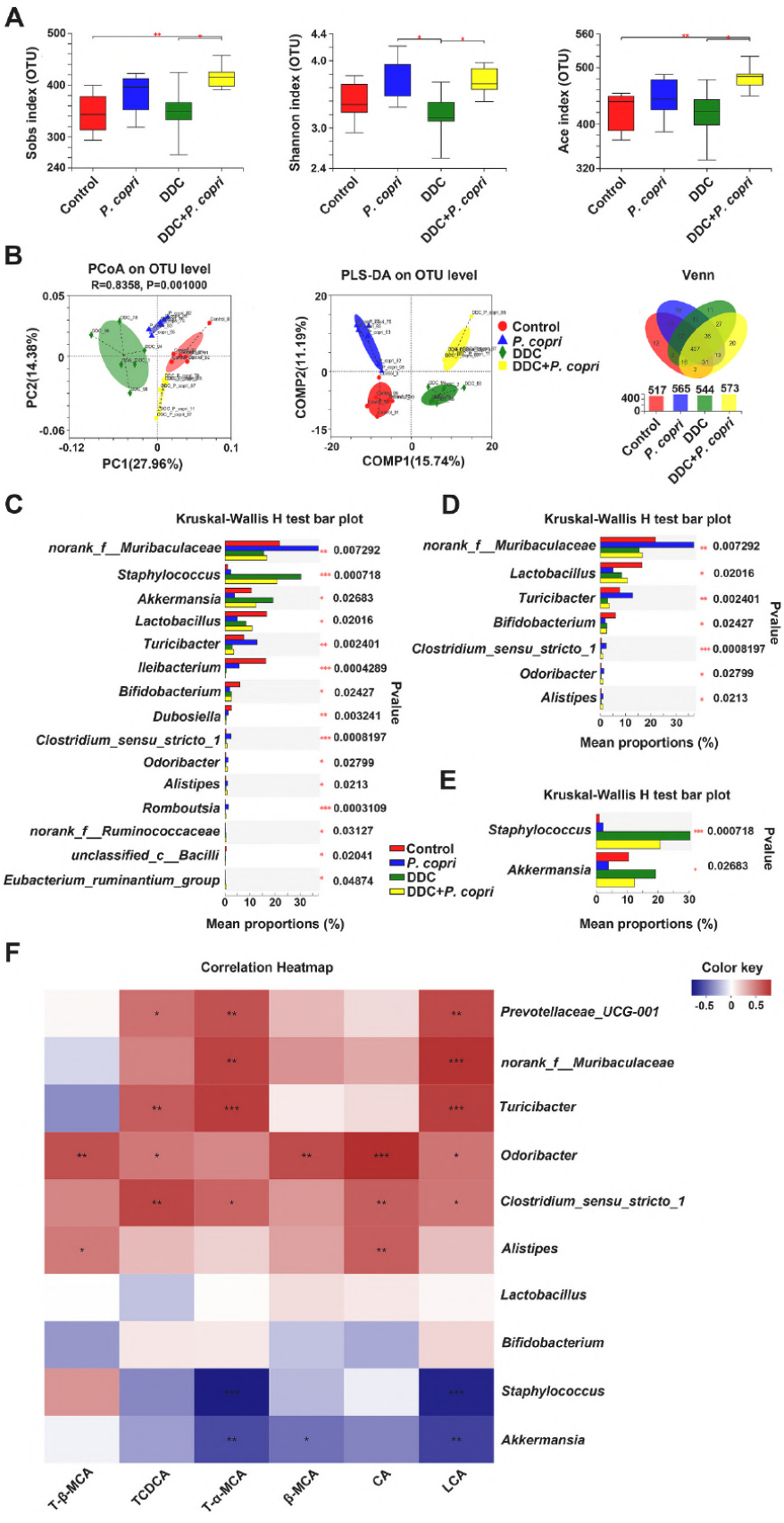

Fig. 5. Faecal samples from each mouse were collected for 16S rRNA sequencing analysis, and the data were stored and interactive analysed on the I-Sanger Bio-cloud platform by Shanghai Majorbio Bio-pharm Technology Co. Ltd. Finally, the platform's two-matrix correlation heat map tool was used to analyse the correlation heat map between the difference quantity table of bacteria and the content data of targeted BAs detection. (A) Student's *t*-test was used to obtain Sobs, Shannon and Ace indexes to analyse intestinal microbial diversity to reflect species diversity and richness. (B) PCoA evaluation showed microbiome variation in the four groups based on abund_jaccard at the OTU level. The classification and intestinal microbial composition of the four groups were analysed based on PLS-DA. The number of common and unique OTUs in multiple groups is presented in a Venn diagram. (C) Kruskal-Wallis rank sum test, FDR multiple test correction, and Tukey-Kramer post hoc test (giving a 95% confidence interval for the mean) were used to detect the top 15 bacterial genera with differential abundances in the microbial community at the genus level in the four treatment groups. (D) Bacterial genera whose abundance decreased significantly after DDC treatment compared with that in the control group, but their composition recovered to some extent after *Prevotella copri* intervention. (E) Genera whose OTU number obviously increased after DDC induction compared with that in the control group but whose abundance was reduced to a certain extent after *P. copri* treatment. (F) Spearman correlation heatmap analysis was conducted between the bacterial genera screened out in D and E and the six selected BAs in Fig. 3E, F. $^{*}p < 0.05$, $^{**}p < 0.01$, $^{***}p < 0.001$; $n = 6$.

$p = 0.003$; $r = -0.45$, $p = 0.03$; $r = -0.60$, $p = 0.002$, respectively). However, *Lactobacillus* and *Bifidobacterium* induced no significant differences among the six BAs. Combined with the changes of the contents of various BAs (Fig. 3E and F), it can be concluded that *P. copri* intervention increased intestinal microbiota transform and synthesize BAs. Among them, there are three kinds of BAs regulated by most genera, namely TCDCA, T-MCA and LCA. As a result, the combined action of the overall intestinal microbiota showed an increase in the level of BA, which directly balanced the state of BA deficiency induced by DDC in the intestinal tract.

4. Discussion

This study explored the unknown pathologic mechanism of PSC by using 0.1% (w/w) DDC to construct obvious bile duct injury, liver injury, and cholestasis in mice. Many studies have proposed that the risk of PSC may be triggered by antigens of microbial origin, or damage caused by disturbances in the intestinal microbiota based on common complication in PSC-IBD patients [8,47,48]. A previous study demonstrated that the abundance of *P. copri* was inhibited in PSC patients and was negatively associated with PSC [11]. Another study confirmed that administration of *P. copri* could increase liver glycogen by regulating BA metabolism in a type 2 diabetes mouse model [20]. Therefore, we speculated that *P. copri* supplementation could alleviate the disease effects in the PSC model. To verify this hypothesis, we administered *P. copri* to mice in control and DDC-supplemented groups, as shown in Fig. 2A. Unfortunately, oral administration of *P. copri* did not improve DDC-diet induced weight loss (Fig. 2C) or liver inflammation (Fig. 2E, F), which was consistent with the proinflammatory effect of this bacterial strain that has been widely reported in arthritis and colitis [36,49–52]. On the other hand, mice were fed diets supplemented with 0.1% DDC throughout the experiment to induce PSC model by inhibiting iron chelatase, leading to the accumulation of protoporphyrin IX (PpIX) in hepatocytes, bile canaliculi, and bile ducts. These might the reason that *P. copri* did not have a good effect on the improvement of this persistent drug-induced injury. Through pathological analysis and evaluation of the expression of inflammatory factors, the addition of *P. copri* was not found to cause an inflammatory response under healthy and normal feeding conditions. However, after DDC treatment, the intestinal mucosa was damaged (Fig. S1C), increasing the risk of bacteria entering the intestinal environment and resulting in liver inflammation in mice in the DDC + *P. copri* group that was still serious. Therefore, we believe that the proinflammatory effect of *P. copri* is likely to occur in conjunction with intestinal damage.

Intestinal bacteria play an intermediate role in the dissociation of conjugated BAs, which is crucial for maintaining intestinal metabolic homeostasis [46,53]. In this study, intervention with *P. copri* resulted in significant differences in the intestinal microbiota in each group, from which we found bacteria genus that had synergistic or antagonistic effects with *P. copri*, and conducted correlation studies with conjugated and unconjugated BAs, as shown in Fig. 5F. The increase in *Prevotellaceae*, *Muribaculaceae* (family *S24–7*) and *Clostridium* was concomitant with the elevation in TCDCA, T-α-MCA and LCA in treatment groups, indicating that administration of *P. copri* might promote TCDCA, T-α-MCA and LCA production by enriching *Muribaculaceae* and *Clostridium* abundance. *Muribaculaceae* can promote expression of the BA transporter *Mdr1* and regulate the TCDCA and T-α-MCA content in mice after partial hepatectomy [54]. Additionally, a previous study certified that the abundance of *Clostridium*, a typical producer of bile salt hydrolase, was positively correlated with *Shp* expression and negatively correlated with *Cyp7a1* expression [55]. These data provide further evidence that the increase in *S24–7* and *Clostridium* might offset cholestasis in the DDC + *P. copri* group by improving BA transport and inhibiting BA synthesis. Conversely, we found that *Staphylococcus* and *Akkermansia* had distinct negative correlations with both T-α-MCA and LCA in the treatment groups. *Staphylococcus* and *Akkermansia* are two important bacteria that contain 7α-dehydroxylation- and deconjugation-related enzymes and BA-related proteins, such as BA transporters, linear amide C—N hydrolases, and cholylglycine hydrolase, to catalyse the unconjugation of conjugated BAs to form free BAs and participate in the transport of BAs. Therefore, we believe that the screened differentially abundant bacterial genera associated with *P. copri* co-acted on BA metabolism, and the three BAs with the closest correlation were identified as TCDCA, T-α-MCA and LCA. According to existing studies, T-α-MCA is a natural endogenous FXR inhibitor [43], and CA can activate FXR [45,46]. Notably, intestinal *Fxr* expression was reversed with changes in T-α-MCA levels, and the combination of CA expression could explain the changes in intestinal *Fxr*. As a result, our data showed that *P. copri* treatment did not affect intestinal *Fxr* due to the reverse function of T-α-MCA and CA (Fig. 3 E, F). In contrast, the activation of CA was apparently superior to the inhibitory effect of T-α-MCA in the DDC + *P. copri* group, thus stimulating a large amount of *Fxr* expression in the SI. Due to the contribution of gut microbiota, *P. copri* intervention could ameliorate cholestasis by controlling the activity of BA receptors (mainly FXR) to regulate the transformation and content of BAs and ultimately improve the metabolism of BAs.

In addition to the significant improvement in cholestasis after intervention with *P. copri* on the background of DDC, the effective reduction in DDC-induced fibrosis by *P. copri* in this experiment was a welcome phenotype. Based on the principle that DDC causes bile duct obstruction and leads to chronic cholestasis, which then develops into inflammation and fibrosis [30], we hypothesize that the elimination of intrahepatic cholestasis is conducive to reversal of fibrosis. Similarly, in a previous study, intervention with the probiotic *Lactobacillus rhamnosus GG (LGG)* significantly attenuated inflammation and liver fibrosis in bile duct ligation (BDL) and Mdr2$^{-/-}$ model mice [56]. In our study, *P. copri* treatment on a DCC background increased the number of *Lactobacillus*, but the number was still lower than that in the control group, which could explain the failure of *P. copri* to completely recover DDC-induced inflammation. In addition, previous studies have suggested that cholestasis can cause extensive bile duct hyperplasia and the formation of portal vein fibrosis in rats and that liver fibrosis can be effectively eliminated within three weeks after the obstruction is relieved, which is in accordance with our experimental results [57]. This suggests that in our study cholestasis and liver fibrosis caused by bile duct obstruction can be gradually recovered after intervention with *P. copri*, which also indirectly reflects the gradual recovery of intrahepatic bile duct obstruction caused by DDC. The reduction in cholestasis and fibrosis is the highlight of this research, but the damage caused by DDC was not completely restored to normal by the effects of *P. copri*.

In conclusion, the present study indicates that *P. copri* can significantly improve DDC-induced cholestasis and liver fibrosis by regulating the metabolism and transport pathways of BAs via combination with intestinal microbiota and especially the FXR signalling pathway. This provides a more comprehensive exploration of *P. copri* and reflects the great significance of *P. copri* in the treatment of chronic cholestasis diseases. By 16S rRNA analysis, we identified bacterial genera that may have synergistic or antagonistic effects with *P. copri*, as well as three BAs, TCDCA, T-α-MCA and LCA that are significantly related to these genera. Although 16S rRNA analysis of gut microbiota is probably not sensitive enough to unambiguously assess bacterial diversity, deeper DNA sequence analysis are required to confirm our finding, we believe this observation lays a foundation for further study of the mutual transformation of BAs under the action of *P. copri*.

CRediT authorship contribution statement

Baorong Jiang: Data curation, Formal analysis, Methodology, Software, Writing – original draft. **Gehui Yuan:** Data curation, Software. **Jialin Wu:** Data curation, Methodology. **Qian Wu:** Formal analysis, Methodology. **Lei Li:** Conceptualization, Formal analysis, Funding acquisition, Resources, Supervision, Project administration, Validation,

Writing – original draft. **Ping Jiang:** Conceptualization, Formal analysis, Funding acquisition, Methodology, Resources, Supervision, Project administration, Validation, Visualization, Writing – original draft.

Declaration of competing interest

The authors declare that they have no known competing financial interests or personal relationships that could have appeared to influence the work reported in this paper.

Acknowledgements

This work was supported by the National Natural Science Foundation of China (no. 82003504 and no. 81973096); The Natural Science Foundation of the Jiangsu Higher Education Institutions of China (no. 19KJB330004); and Science and Technology Development Fund of Nanjing Medical University (no. NMUB2019012).

Appendix A. Supplementary data

Supplementary data to this article can be found online at https://doi.org/10.1016/j.bbadis.2021.166320.

References

[1] J.E. Eaton, J.A. Talwalkar, K.N. Lazaridis, G.J. Gores, K.D. Lindor, Pathogenesis of primary sclerosing cholangitis and advances in diagnosis and management, Gastroenterology 145 (2013) 521–536.
[2] M. Pinzani, T.V. Luong, Pathogenesis of biliary fibrosis, Biochim. Biophys. Acta Mol. Basis Dis. 2018 (1864) 1279–1283.
[3] B.K. Chung, T.H. Karlsen, T. Folseraas, Cholangiocytes in the pathogenesis of primary sclerosing cholangitis and development of cholangiocarcinoma, Biochim. Biophys. Acta Mol. Basis Dis. 2018 (1864) 1390–1400.
[4] K. Tsuneyama, N. Kono, M. Yamashiro, W. Kouda, A. Sabit, M. Sasaki, Y. Nakanuma, Aberrant expression of stem cell factor on biliary epithelial cells and peribiliary infiltration of c-kit-expressing mast cells in hepatolithiasis and primary sclerosing cholangitis: a possible contribution to bile duct fibrosis, J. Pathol. 189 (1999) 609–614.
[5] A.A. Gossard, J.A. Talwalkar, Cholestatic liver disease, Med Clin North Am 98 (2014) 73–85.
[6] J.K. Dyson, U. Beuers, D.E.J. Jones, A.W. Lohse, M. Hudson, Primary sclerosing cholangitis, Lancet 391 (2018) 2547–2559.
[7] T.H. Karlsen, T. Folseraas, D. Thorburn, M. Vesterhus, Primary sclerosing cholangitis - a comprehensive review, J. Hepatol. 67 (2017) 1298–1323.
[8] M. Irles-Depe, S. Roullet, M. Neau-Cransac, J. Dumortier, S. Dharancy, P. Houssel-Debry, O. Boillot, L. Chiche, C. Laurent, D. Laharie, V. De Ledinghen, Impact of preexisting inflammatory bowel disease on the outcome of liver transplantation for primary sclerosing cholangitis, Liver Transpl. 26 (2020) 1477–1491.
[9] F. Pallavicino, R. Pellicano, S. Reggiani, D. Simondi, C. Sguazzini, A.G. Bonagura, F. Cisaro, M. Rizzetto, M. Astegiano, Inflammatory bowel diseases and primary sclerosing cholangitis: hepatic and pancreatic side effects due to azathioprine, Eur. Rev. Med. Pharmacol. Sci. 17 (2013) 84–87.
[10] D. Ellinghaus, T. Folseraas, K. Holm, E. Ellinghaus, E. Melum, T. Balschun, J. K. Laerdahl, A. Shiryaev, D.N. Gotthardt, T.J. Weismuller, C. Schramm, M. Wittig, A. Bergquist, E. Bjornsson, H.U. Marschall, M. Vatn, A. Teufel, C. Rust, C. Gieger, H.E. Wichmann, H. Runz, M. Sterneck, C. Rupp, F. Braun, R.K. Weersma, C. Wijmenga, C.Y. Ponsioen, C.G. Mathew, P. Rutgeerts, S. Vermeire, E. Schrumpf, J.R. Hov, M.P. Manns, K.M. Boberg, S. Schreiber, A. Franke, T.H. Karlsen, Genome-wide association analysis in primary sclerosing cholangitis and ulcerative colitis identifies risk loci at GPR35 and TCF4, Hepatology 58 (2013) 1074–1083.
[11] L. Bajer, M. Kverka, M. Kostovcik, P. Macinga, J. Dvorak, Z. Stehlikova, J. Brezina, P. Wohl, J. Spicak, P. Drastich, Distinct gut microbiota profiles in patients with primary sclerosing cholangitis and ulcerative colitis, World J. Gastroenterol. 23 (2017) 4548–4558.
[12] S. Vieira-Silva, J. Sabino, M. Valles-Colomer, G. Falony, G. Kathagen, C. Caenepeel, I. Cleynen, S. van der Merwe, S. Vermeire, J. Raes, Quantitative microbiome profiling disentangles inflammation- and bile duct obstruction-associated microbiota alterations across PSC/IBD diagnoses, Nat. Microbiol. 4 (2019) 1826–1831.
[13] M. Kummen, K. Holm, J.A. Anmarkrud, S. Nygard, M. Vesterhus, M.L. Hoivik, M. Troseid, H.U. Marschall, E. Schrumpf, B. Moum, H. Rosjo, P. Aukrust, T. H. Karlsen, J.R. Hov, The gut microbial profile in patients with primary sclerosing cholangitis is distinct from patients with ulcerative colitis without biliary disease and healthy controls, Gut 66 (2017) 611–619.
[14] M.N. Quraishi, A. Acharjee, A.D. Beggs, R. Horniblow, C. Tselepis, G. Gkoutos, S. Ghosh, A.E. Rossiter, N. Loman, W. van Schaik, D. Withers, J.R.F. Walters, G. M. Hirschfield, T.H. Iqbal, A pilot integrative analysis of colonic gene expression, gut microbiota, and immune infiltration in primary sclerosing cholangitis-inflammatory bowel disease: association of disease with bile acid pathways, J Crohns Colitis 14 (2020) 935–947.
[15] A. Tett, K.D. Huang, F. Asnicar, H. Fehlner-Peach, E. Pasolli, N. Karcher, F. Armanini, P. Manghi, K. Bonham, M. Zolfo, F. De Filippis, C. Magnabosco, R. Bonneau, J. Lusingu, J. Amuasi, K. Reinhard, T. Rattei, F. Boulund, L. Engstrand, A. Zink, M.C. Collado, D.R. Littman, D. Eibach, D. Ercolini, O. Rota-Stabelli, C. Huttenhower, F. Maixner, N. Segata, The prevotella copri complex comprises four distinct clades underrepresented in westernized populations, Cell Host Microbe 26 (2019) 666–679 e667.
[16] R.E. Ley, Gut microbiota in, Prevotella in the gut: choose carefully, Nat. Rev. Gastroenterol. Hepatol. 13 (2016) (2015) 69–70.
[17] P. Kovatcheva-Datchary, A. Nilsson, R. Akrami, Y.S. Lee, F. De Vadder, T. Arora, A. Hallen, E. Martens, I. Bjorck, F. Backhed, Dietary fiber-induced improvement in glucose metabolism is associated with increased abundance of prevotella, Cell Metab. 22 (2015) 971–982.
[18] F. De Filippis, E. Pasolli, A. Tett, S. Tarallo, A. Naccarati, M. De Angelis, E. Neviani, L. Cocolin, M. Gobbetti, N. Segata, D. Ercolini, Distinct genetic and functional traits of human intestinal prevotella copri strains are associated with different habitual diets, Cell Host Microbe 25 (2019) 444–453 e443.
[19] P.J. Vuillermin, M. O'Hely, F. Collier, K.J. Allen, M.L.K. Tang, L.C. Harrison, J. B. Carlin, R. Saffery, S. Ranganathan, P.D. Sly, L. Gray, J. Molloy, A. Pezic, M. Conlon, D. Topping, K. Nelson, C.R. Mackay, L. Macia, J. Koplin, S.L. Dawson, M. Moreno-Betancur, A.L. Ponsonby, J.C.V Institute, B.I.S.I. Group, Maternal carriage of Prevotella during pregnancy associates with protection against food allergy in the offspring, Nat Commun 11 (2020) 1452.
[20] N. Pean, A. Le Lay, F. Brial, J. Wasserscheid, C. Rouch, M. Vincent, A. Myridakis, L. Hedjazi, M.E. Dumas, E. Grundberg, M. Lathrop, C. Magnan, K. Dewar, D. Gauguier, Dominant gut prevotella copri in gastrectomised non-obese diabetic goto-kakizaki rats improves glucose homeostasis through enhanced FXR signalling, Diabetologia 63 (2020) 1223–1235.
[21] J. Li, P.A. Dawson, Animal models to study bile acid metabolism, Biochim. Biophys. Acta Mol. Basis Dis. 2019 (1865) 895–911.
[22] B. Sanchez, Bile acid-microbiota crosstalk in gastrointestinal inflammation and carcinogenesis: a role for bifidobacteria and lactobacilli? Nat. Rev. Gastroenterol. Hepatol. 15 (2018) 205.
[23] A. Wahlstrom, S.I. Sayin, H.U. Marschall, F. Backhed, Intestinal crosstalk between bile acids and microbiota and its impact on host metabolism, Cell Metab. 24 (2016) 41–50.
[24] J.Y. Chiang, Bile acids: regulation of synthesis, J. Lipid Res. 50 (2009) 1955–1966.
[25] A. Wahlstrom, S.I. Sayin, H.U. Marschall, F. Backhed, Intestinal crosstalk between bile acids and microbiota and its impact on host metabolism, Cell Metab. 24 (2016) 41–50.
[26] W.A. Alrefai, R.K. Gill, Bile acid transporters: structure, function, regulation and pathophysiological implications, Pharm. Res. 24 (2007) 1803–1823.
[27] R.F. Kunst, H.J. Verkade, R.P.J. Oude Elferink, S.F.J. van de Graaf, Targeting the four pillars of enterohepatic bile salt cycling; lessons from genetics and pharmacology, Hepatology (2020).
[28] P.J. Meier, B. Stieger, Bile salt transporters, Annu. Rev. Physiol. 64 (2002) 635–661.
[29] G.A. Kullak-Ublick, B. Stieger, P.J. Meier, Enterohepatic bile salt transporters in normal physiology and liver disease, Gastroenterology 126 (2004) 322–342.
[30] P. Fickert, U. Stoger, A. Fuchsbichler, T. Moustafa, H.U. Marschall, A.H. Weiglein, O. Tsybrovskyy, H. Jaeschke, K. Zatloukal, H. Denk, M. Trauner, A new xenobiotic-induced mouse model of sclerosing cholangitis and biliary fibrosis, Am. J. Pathol. 171 (2007) 525–536.
[31] K. Chaudhary, C. Liedtke, S. Wertenbruch, C. Trautwein, K.L. Streetz, Caspase 8 differentially controls hepatocytes and non-parenchymal liver cells during chronic cholestatic liver injury in mice, J. Hepatol. 59 (2013) 1292–1298.
[32] T. Pradhan-Sundd, R. Vats, J.O. Russell, S. Singh, A.A. Michael, L. Molina, S. Kakar, P. Cornuet, M. Poddar, S.C. Watkins, K.N. Nejak-Bowen, S.P. Monga, P. Sundd, Dysregulated bile transporters and impaired tight junctions during chronic liver injury in mice, Gastroenterology 155 (2018) 1218–1232 e1224.
[33] A. Fragoulis, J. Schenkel, M. Herzog, T. Schellenberg, H. Jahr, T. Pufe, C. Trautwein, T.W. Kensler, K.L. Streetz, C.J. Wruck, Nrf2 ameliorates DDC-induced sclerosing cholangitis and biliary fibrosis and improves the regenerative capacity of the liver, Toxicol. Sci. 169 (2019) 485–498.
[34] Y. Yamazaki, R. Moore, M. Negishi, Nuclear receptor CAR (NR1I3) is essential for DDC-induced liver injury and oval cell proliferation in mouse liver, Lab. Investig. 91 (2011) 1624–1633.
[35] V. Mariotti, M. Strazzabosco, L. Fabris, D.F. Calvisi, Animal models of biliary injury and altered bile acid metabolism, Biochim. Biophys. Acta Mol. Basis Dis. 2018 (1864) 1254–1261.
[36] C. Yu, B. Zhou, X. Xia, S. Chen, Y. Deng, Y. Wang, L. Wu, Y. Tian, B. Zhao, H. Xu, L. Yang, Prevotella copri is associated with carboplatin-induced gut toxicity, Cell Death Dis. 10 (2019) 714.
[37] C. An, J. Wen, Z. Hu, W.E. Mitch, Y. Wang, Phosphoinositide 3-kinase gamma deficiency attenuates kidney injury and fibrosis in angiotensin II-induced hypertension, Nephrol. Dial. Transplant. 35 (2020) 1491–1500.
[38] U.C. Dadwal, A.R. Merkel, J.M. Page, K.A. Kwakwa, M. Kessler, J.A. Rhoades, 3D bone morphology alters gene expression, motility, and drug responses in bone metastatic tumor cells, Int. J. Mol. Sci. 21 (2020).
[39] M.M. Nielsen, K.L. Lambertsen, B.H. Clausen, M. Meyer, D.R. Bhandari, S.T. Larsen, S.S. Poulsen, B. Spengler, C. Janfelt, H.S. Hansen, Mass spectrometry imaging of biomarker lipids for phagocytosis and signalling during focal cerebral ischaemia, Sci. Rep. 6 (2016) 39571.

[40] P. Li, G. Wu, Roles of dietary glycine, proline, and hydroxyproline in collagen synthesis and animal growth, Amino Acids 50 (2018) 29–38.
[41] M.K. Gordon, R.A. Hahn, Collagens, Cell Tissue Res. 339 (2010) 247–257.
[42] S. Udenfriend, Formation of hydroxyproline in collagen, Science 152 (1966) 1335–1340.
[43] S.I. Sayin, A. Wahlstrom, J. Felin, S. Jantti, H.U. Marschall, K. Bamberg, B. Angelin, T. Hyotylainen, M. Oresic, F. Backhed, Gut microbiota regulates bile acid metabolism by reducing the levels of tauro-beta-muricholic acid, a naturally occurring FXR antagonist, Cell Metab. 17 (2013) 225–235.
[44] Y.C. Qi, G.Z. Duan, W. Mao, Q. Liu, Y.L. Zhang, P.F. Li, Taurochenodeoxycholic acid mediates cAMP-PKA-CREB signaling pathway, Chin, J. Nat. Med. 18 (2020) 898–906.
[45] L. Ding, L. Yang, Z. Wang, W. Huang, Bile acid nuclear receptor FXR and digestive system diseases, Acta Pharm. Sin. B 5 (2015) 135–144.
[46] W. Jia, G. Xie, W. Jia, Bile acid-microbiota crosstalk in gastrointestinal inflammation and carcinogenesis, Nat. Rev. Gastroenterol. Hepatol. 15 (2018) 111–128.
[47] J.L. Damman, E.A. Rodriguez, A.H. Ali, C.W. Buness, K.L. Cox, E.J. Carey, K. D. Lindor, Review article: the evidence that vancomycin is a therapeutic option for primary sclerosing cholangitis, Aliment. Pharmacol. Ther. 47 (2018) 886–895.
[48] K. Conrad, D. Roggenbuck, M.W. Laass, Diagnosis and classification of ulcerative colitis, Autoimmun. Rev. 13 (2014) 463–466.
[49] D. Alpizar-Rodriguez, T.R. Lesker, A. Gronow, B. Gilbert, E. Raemy, C. Lamacchia, C. Gabay, A. Finckh, T. Strowig, Prevotella copri in individuals at risk for rheumatoid arthritis, Ann. Rheum. Dis. 78 (2019) 590–593.
[50] A. Pianta, S. Arvikar, K. Strle, E.E. Drouin, Q. Wang, C.E. Costello, A.C. Steere, Evidence of the immune relevance of prevotella copri, a gut microbe, patients with rheumatoid arthritis, arthritis, Rheumatol 69 (2017) 964–975.
[51] N. Rolhion, B. Chassaing, M.A. Nahori, J. de Bodt, A. Moura, M. Lecuit, O. Dussurget, M. Berard, M. Marzorati, H. Fehlner-Peach, D.R. Littman, A. T. Gewirtz, T. Van de Wiele, P. Cossart, A listeria monocytogenes bacteriocin can target the commensal prevotella copri and modulate intestinal infection, Cell Host Microbe 26 (2019) 691–701 e695.
[52] J.U. Scher, A. Sczesnak, R.S. Longman, N. Segata, C. Ubeda, C. Bielski, T. Rostron, V. Cerundolo, E.G. Pamer, S.B. Abramson, C. Huttenhower, D.R. Littman, Expansion of intestinal prevotella copri correlates with enhanced susceptibility to arthritis, elife 2 (2013), e01202.
[53] S.L. Long, C.G.M. Gahan, S.A. Joyce, Interactions between gut bacteria and bile in health and disease, Mol. Asp. Med. 56 (2017) 54–65.
[54] H.X. Liu, C.S. Rocha, S. Dandekar, Y.J. Wan, Functional analysis of the relationship between intestinal microbiota and the expression of hepatic genes and pathways during the course of liver regeneration, J. Hepatol. 64 (2016) 641–650.
[55] W.W. Wang, J. Wang, H.J. Zhang, S.G. Wu, G.H. Qi, Supplemental clostridium butyricum modulates lipid metabolism through shaping gut microbiota and bile acid profile of aged laying hens, Front. Microbiol. 11 (2020) 600.
[56] Y. Liu, K. Chen, F. Li, Z. Gu, Q. Liu, L. He, T. Shao, Q. Song, F. Zhu, L. Zhang, M. Jiang, Y. Zhou, S. Barve, X. Zhang, C.J. McClain, W. Feng, Probiotic lactobacillus rhamnosus GG prevents liver fibrosis through inhibiting hepatic bile acid synthesis and enhancing bile acid excretion in mice, Hepatology 71 (2020) 2050–2066.
[57] G. Abdel-Aziz, G. Lebeau, P.Y. Rescan, B. Clement, M. Rissel, Y. Deugnier, J. P. Campion, A. Guillouzo, Reversibility of hepatic fibrosis in experimentally induced cholestasis in rat, Am. J. Pathol. 137 (1990) 1333–1342.